Initial experience of combined microstructural and functional magnetic resonance imaging for the characterisation of renal tumours.

Richard Hesketh[1], Timothy Bray[1], Snigdha Sen[2], Lorna Smith[1], Rafat Chowdhury[1], Adam Retter[1], Lucy Caselton[1], David Atkinson[1], Eleftheria Panagiotaki[2], Fiona Gong[1], Max Bullock[1], Joey Clemente[1], Maxine Tran[3], and Shonti Punwani[1]
[1]Centre for Medical Imaging, University College London, London, United Kingdom, [2]Centre for Medical Imaging Computing, UCL, London, United Kingdom, [3]Department of Surgical Biotechnology, UCL, London, United Kingdom

Synopsis

Keywords: Kidney, Cancer, Hyperpolarised MRI, renal cancer, VERDICT

Motivation: Accurate differentiation of renal tumour subtype and grade is not currently possible using standard of care imaging.

Goal(s): To use combined functional and microstructural MRI in the form of diffusion weighted imaging with VERDICT, proton density fat fraction and hyperpolarised [1-13C]pyruvate to detect the different histological and metabolic features of different renal tumours.
Two patients with histologically proven renal tumours (grade 2 clear cell and grade 3 papillary) underwent MRI imaging.

Approach: Two patients with histologically proven renal tumours (grade 2 clear cell and grade 3 papillary) underwent MRI imaging.

Results: Combined function and microstructural MRI differentiated tumour types and normal kidney.

Impact: This study demonstrates the first combined use of VERDICT, PDFF and hyperpolarised [1-13C]pyruvate. The differentiation of renal tumours has proven difficult on imaging and this combination is a promising approach to this significant clinical problem.

Background

Renal cancer has the highest mortality rate of any urological cancer with over 430,000 new cases every year. Survival is dependent on stage – localised disease has a 5-year survival rate of 93% which falls to 12% for metastatic disease. Consequently, radical nephrectomy was recommended for all solid renal tumours until relatively recently. However, though the increased incidence of small renal tumours, around 15% of tumours are benign and only ~2% of malignant tumours have metastatic potential1. Furthermore, renal tumours demonstrate considerable intra-lesional genetic, metabolic and morphological heterogeneity meaning that biopsy is not routinely recommended2. Current standard of care imaging cannot differentiate between tumour types and grade with sufficient specificity and specificity, therefore management of small renal tumours is currently decided by shared decision making between clinician and patient, informed by population rather than personalised risk of progression.However, different renal tumours subtypes demonstrate markedly different histopathological features, specifically cell size, cell density, vascularity, stromal space and intracellular lipid content vary between subtypes and grades3. Furthermore, cellular metabolism also varies between tumours, for example benign oncocytomas are characterised by high numbers of partially defective mitochondria and hypoxia inducible factor (HIF) 1-alpha inhibition leading to glycolytic flux into the TCA cycle and accumulation of TCA cycle metabolites, particularly alpha-ketoglutarate4. Conversely, HIF activation secondary to vHL loss leads to increased glycolysis and lactate production and decreased TCA cycle flux, a feature of most clear cell renal cell carcinomas5. We hypothesised that renal tumour grade and subtype could be differentiated using a combination of of quantitative microstructural and functional MRI and present our preliminary results using vascular, extracellular and restricted diffusion for cytometry in tumours (VERDICT)6, proton density fat-fraction (PDFF)7 and hyperpolarised MRI following injection of [1-13C]pyruvate in renal tumours.

Methods

Patients provided written informed consent. Microstructural MRI was performed on a 3T Ingenia MRI scanner (Philips Healthcare). T2-weighted imaging was acquired in two planes. For VERDICT MRI diffusion weighted images were acquired using a pulsed-gradient spin-echo sequence with EPI readout in the coronal plane with a, TR 2000-3349 ms, TE 54-87 ms, FoV 220 x 220 mm, matrix of 176 x 176, voxel size 1.25 x 1.25 x 5 mm and b values of 70, 90, 150, 500, 1000, 1500, 2000, 2200 and 2500 s/mm2. Four signal averages were collected for b70 – b150, 6 for b500-b1500 and 8 for b2000-b2500.PDFF imaging was performed using a gradient echo sequence (mDixon Quant, Philips Healthcare). Single breathold acquisition was performed with a flip angle of 5°, TR 6.39 ms, six echoes acquired at even intervals between 1.089 – 5.191 ms, acquisition matrix of 160 x 160, FoV of 250 x 160 mm and slice thickness of 2.5 mm. Water only, fat only, fat fraction and T2* maps were derived using vendor-supplied software, and PDFF values calculated for normal kidney and tumour. Hyperpolarised MRI[1-13C]pyruvic acid was hyperpolarised as previously described in a clinical hyperpolarised (SpinLab, GE Healthcare) and 40 mL injected intravenously. MRI was performed using a 3T Biograph PET-MRI (Siemens). A single slice multi-echo bSSFP sequence8 with an FoV: 300 x 300 x 30 mm, acquisition matrix: 16 x 16; flip angle: 30°, TR: 15.8 ms, dTE: 1.1 ms 11 echoes, and 12 signal averages, with retrospective multipoint IDEAL metabolite separation.

Results

Two patients with RCC were imaged. One patient had a 7 cm T1b N0 M0 grade 2 (low grade) clear cell RCC (ccRCC), the other had a 3.2 cm T1a N0 M1 grade 3 (high grade) papillary RCC (pRCC). PDFF values were 1.1 ± 6.0% (normal kidney), 8.4 ± 5.0% (ccRCC) and 0.26 ± 3.7% (pRCC) (Fig. 1c & d).VERDICT measurements of intracellular volume fraction (fIC) were elevated in both tumours relative to normal kidney and highest in pRCC while intravascular volume fraction (fVasc) of normal renal cortex and both tumours were similar to the enhancement demonstrated on CT (Fig. 1e & f).Following injection of hyperpolarised [1-13C]pyruvate both [1-13C]lactate and [1-13C]alanine were detected in the tumour region, with a tumour lactate:pyruvate ratio of 0.15 and kPL 0.002 (Fig. 2).

Conclusion

We present the first application of combined quantitative microstructural and functional MRI of renal tumours using hyperpolarised [1-13C]pyruvate, PDFF and VERDICT MRI. In the imaged ccRCC, fat fraction and kPL were similar to previous reports9, 10.

Acknowledgements

No acknowledgement found.

References

References 1. Smaldone MC, Kutikov A, Egleston BL, Canter DJ, Viterbo R, Chen DY, et al. Small renal masses progressing to metastases under active surveillance: a systematic review and pooled analysis. Cancer. 2012;118(4):997-1006.

2. Ueno D, Xie Z, Boeke M, Syed J, Nguyen KA, McGillivray P, et al. Genomic Heterogeneity and the Small Renal Mass. Clin Cancer Res. 2018;24(17):4137-44.

3. Muglia VF, Prando A. Renal cell carcinoma: histological classification and correlation with imaging findings. Radiol Bras. 2015;48(3):166-74.

4. De Luise M, Girolimetti G, Okere B, Porcelli AM, Kurelac I, Gasparre G. Molecular and metabolic features of oncocytomas: Seeking the blueprints of indolent cancers. Biochim Biophys Acta Bioenerg. 2017;1858(8):591-601.

5. Bacigalupa ZA, Rathmell WK. Beyond glycolysis: Hypoxia signaling as a master regulator of alternative metabolic pathways and the implications in clear cell renal cell carcinoma. Cancer Lett. 2020;489:19-28.

6. Panagiotaki E, Chan RW, Dikaios N, Ahmed HU, O'Callaghan J, Freeman A, et al. Microstructural characterization of normal and malignant human prostate tissue with vascular, extracellular, and restricted diffusion for cytometry in tumours magnetic resonance imaging. Invest Radiol. 2015;50(4):218-27.

7. Bray TJP, Bainbridge A, Punwani S, Ioannou Y, Hall-Craggs MA. Simultaneous Quantification of Bone Edema/Adiposity and Structure in Inflamed Bone Using Chemical Shift-Encoded MRI in Spondyloarthritis. Magn Reson Med. 2018;79(2):1031-42.

8. Muller CA, Hundshammer C, Braeuer M, Skinner JG, Berner S, Leupold J, et al. Dynamic 2D and 3D mapping of hyperpolarized pyruvate to lactate conversion in vivo with efficient multi-echo balanced steady-state free precession at 3 T. NMR Biomed. 2020;33(6):e4291.

9. Zhang Y, Udayakumar D, Cai L, Hu Z, Kapur P, Kho EY, et al. Addressing metabolic heterogeneity in clear cell renal cell carcinoma with quantitative Dixon MRI. JCI Insight. 2017;2(15).

10. Ursprung S, Woitek R, McLean MA, Priest AN, Crispin-Ortuzar M, Brodie CR, et al. Hyperpolarized (13)C-Pyruvate Metabolism as a Surrogate for Tumor Grade and Poor Outcome in Renal Cell Carcinoma-A Proof of Principle Study. Cancers (Basel). 2022;14(2).

Figures

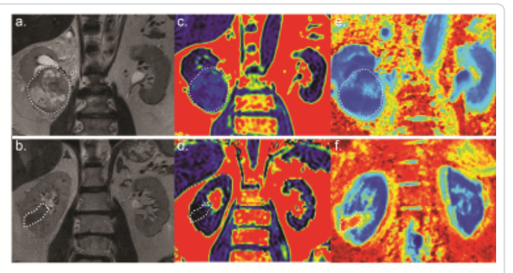

Figure 1. Coronal MRI images of two patients with clear cell RCC (top row) and papillary RCC (bottom row). (a & b) T2-weighted; (c & d) proton density fat fraction; (e & f) VERDICT-derived intracellular volume fraction (fIC).

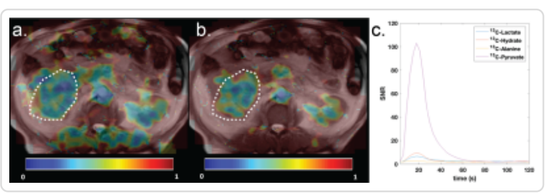

Figure 2. Example hyperpolarised MRI images overlaid on an axial T2W image from the patient with a clear cell RCC. (a) lactate:pyruvate AUC ratio map; (b) alanine:pyruvate AUC ratio map; (c) time course of the different metabolites detected from the tumour ROI.